Biomass Conversion and Biorefinery
https://doi.org/10.1007/s13399-023-05021-y

ORIGINAL ARTICLE

High-efficiency adsorption of heavy metals on sulfur nanoparticles coated biochar derived from alfalfa residues and its biological effects

Neda Seyedi[1] · Mehdi Ahmadyousefi[2] · Neda Seyedi Marghaki[3] · Roya Afsharipour[2,4] · Mohammadjavad Jahanshahi[1] · Mahdieh Amiri Nezhad[5]

Received: 23 August 2023 / Revised: 11 October 2023 / Accepted: 14 October 2023

Abstract

In this study, biochar modified with sulfur nanoparticles (SNPs@BC) was synthesized in terms of providing a low-cost adsorbent for cadmium and lead adsorption. Morphology and structure of SNPs@BC were investigated by scanning electron microscopy (SEM), X-ray diffraction (XRD), and Fourier transform infrared spectroscopy (FT-IR). And also, thermal gravimetric analysis (TGA) was used to study the thermal stability of the synthesized adsorbent. The results indicated that the biochar surface was successfully coated with sulfur nanoparticles and could improve its performance as a soil amendment or an adsorbent. Cadmium and lead adsorption studies on SNPs@BC exhibited high Langmuir cadmium (97 mg/g) and lead (99 mg/g) adsorption capacity, and heavy metal toxicity can be reduced by adsorption of cadmium and lead on SNPs@BC. The seed germination rate and seedling growth in cadmium-lead adsorbed SNPs@BC were the same as in the cadmium-free and lead-free control groups. This study suggests that SNPs@BC can be used as an efficient and eco-friendly sorbent for heavy metal removal.

Keywords Heavy metal adsorption · SNPs@BC · Biological effect · Eco-friendly adsorbent · Wastewater treatment

1 Introduction

The tremendous progress of industrial activity leads to the release of heavy metals such as cadmium (Cd(II)) and lead (Pd(II)) into the environment and the contamination of water sources and soil [1, 2]. These metals are not biodegradable and can accumulate in living organisms and cause various ailments, including damage to the central nervous or mental systems, reduced energy levels in the body, and damage to the lungs, liver, and other major organs in human and animals [3, 4]. Low concentrations of Cd(II) and Pd(II) are highly toxic and poisonous to plants and have no part in plants' growth and other metabolic processes. They are primarily collected in the roots, shoots, and edible parts of the plants. Some plants can tolerate a small concentration of them, while some show changes in their phenotype, such as a decrease in weight, roots, and shoot lengths. Cytotoxicity, inflammation, and deterioration have also been observed in plants due to their toxicity [5]. This is why it is so important to develop efficient and cost-effective techniques to remove Cd(II) and Pb(II) ions from water, wastewater, and soil. There are many methods to remove metal ions from aqueous solutions including adsorption, solvent extraction, precipitation, and ion exchange [6–8]. Among the aforementioned methods, adsorption techniques are most often considered due to their simplicity, high selectivity, high efficiency, and low cost [6, 9]. In addition, with these techniques, it is important to select the appropriate sorbent, which directly affects the efficiency of the adsorption method. In this case, biosorbents are more attractive due to the abundance of natural resources and high adsorption efficiency for removing heavy metals from the aqueous environment

✉ Neda Seyedi
nedaseyedi@ujiroft.ac.ir

1 Department of Chemistry, Faculty of Science, University of Jiroft, Jiroft 7867161167, Iran

2 Researcher in University of Jiroft, Jiroft 7867161167, Iran

3 Department of Environmental Health, Faculty of Medical Sciences, Tarbiat Modares University, Tehran, Iran

4 Department of Chemistry, Faculty of Science, Yazd University, Yazd, Iran

5 Department of Agronomy and Plant Breeding, Faculty of Agriculture, University of Jiroft, Jiroft, Iran

Published online: 27 October 2023

and soil [10]. Biochar is the carbonaceous product which produces via the thermal pyrolysis process of organic matter under inert atmosphere conditions [11, 12]. Due to the relative cheapness and universality of feedstock materials such as the wastes of agriculture and forest, biochar is a great candidate for conventional remediation agents for the removal of different contaminates in the environment, especially heavy metals [13–15]. However, biochar has a highly inert surface, which leads to low adsorption capacity for heavy metals. Hence, various modification and activation strategies including surface oxidation, functionalization, and exploration have been employed to improve their efficiency in environmental remediation [16, 17]. As a result of these modifications and activation, the surface sorption sites increased and the ability of biochar for removing contamination improved [18]. The capability of biochar for the immobilization of heavy metals depends on different factors such as the type of feedstock, production methods, and processing conditions [18, 19].

Recently, nanotechnology has been enormously utilized for the remediation of contaminated ground and surface water, sediment, and soil. The nanoparticles are the particles with a size in the range of 1.0–100 nm that possess great reactivity and large surface area than macroparticles for the removal of pollutants [20]. The surface modification of of biochar with sulfur nanoparticles increase their ability to remove of heavy metals from environmental. Moreover, this combination is more noteworthy when the sulfur nanoparticles were synthesized from green materials with great availability.

The survey of previous literatures shows that biochar also has the ability to immobilize heavy metals from contaminated soil and water [16, 21]. In addition, biochar as an effective sorbent possesses of great potential to concentrate toxic heavy metals. Other studies also proved that biochar was employed in soil and water, could decrease the leaching of heavy metals in soil and water, and decrease their absorption by earthworms [22, 23]. However, the biological effects of the heavy metals adsorbed on biochar need to be studied on growing plants.

In this study, the biochar was synthesized from various biomass feedstocks through the thermal pyrolysis processes at 500 °C. The biochar surface was oxidized in the presence of nitric acid. Sulfur nanoparticles were synthesized from rosemary leaves' aqueous extract and then used to modify the biochar surface. This biosorbent was used to remove Cd(II) and Pb(II) ions from wastewater. The effective parameters of the adsorption process, including pH, initial concentration, adsorbent mass, and contact time, have been optimized by the central composite design. In addition, adsorption isotherms and the biological effect of heavy metal-adsorbed biochar on seed germination and plant growth were investigated.

The most important points of this study were (1) the use of different biomass feedstocks for the preparation of biochar and after characterizing; the optimal biochar was chosen for the preparation of final adsorbent (SNPs@BC); (2) rosemary was used to prepare sulfur nanoparticles on the surface of biochar; the presence of sulfur increases the absorption of heavy metals; (3) evaluate the sorption mechanism of heavy metals on SNPs@BC; (4) investigate the effects of cadmium and lead adsorbed biochar on seed germination and rate of plant growth; and (5) assay the capability of biochar of the bioaccumulation of cadmium and lead in plants. The schematic illustration of the synthesis and sorption mechanism was exhibited in Fig. 1.

2 Experimental

2.1 Chemicals and instrumentation

All the used materials were acquired from Merck and Sigma-Aldrich and applied without further purification. Biochar was derived from five types of biomasses from different organic sources including rice straw and stubble, sawdust, alfalfa leaves and stems, potato leaves and stems, and palm leaves. The identification of the functional groups in the adsorbent structure was performed by analysis of FT-IR spectra which were collected using a KBr pellet on a Bruker Tensor 27 Fourier transform infrared spectrometer. To study the deposition of sulfur nanoparticles on biochar, X-ray diffraction device (Panalytical, Almelo, the Netherlands) using Cu Ka radiation (wavelength = 1.54 Å) was used. TGA (STA503, Germany) was used to study the thermal stability of the synthesized sorbent. The morphology of the sorbent was studied by scanning electron microscope (SEM) as well as energy-dispersive X-ray spectroscopy (EDS) (SIGMA VP from Carl Zeiss Inc., Jena, Germany).

2.2 Preparation of leaves' aqueous extract of rosemary

The rosemary leaves were separated, cleaned, and washed carefully with distilled water and dried in the open air at the laboratory. Leave plant extract was obtained according to the present literature available for this plant [24]: dried leaves (20 g) were cut into suitable parts and mixed with 500-mL deionized water and heated at 80 °C for 10 min and then were cooled at room temperature, and the aqueous extract was obtained by filtration and then centrifuged at 1200 rpm to remove solid particles. The filtrate was stored at refrigerator for further experimental tests.

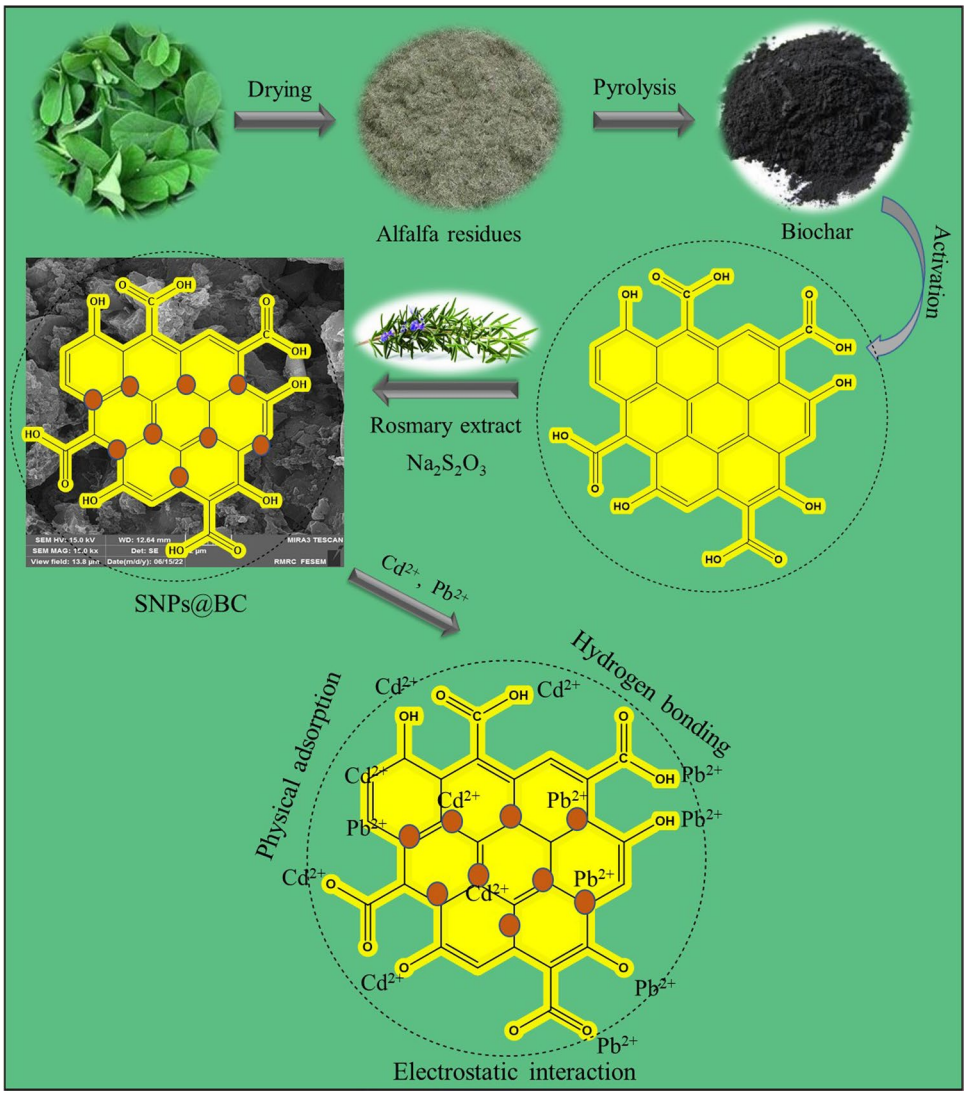

Fig. 1 Schematic illustration of synthesis and sorption mechanism of Cd^{2+} and Pb^{2+}

2.3 Preparation of biochar (BC)

Biochar was derived from five types of biomasses from different organic sources including rice straw and stubble, sawdust, alfalfa leaves and stems, potato leaves and stems, and palm leaves. After preparing and characterizing of biochar (Table S1), the obtained biochar from alfalfa residues at a temperature of 500 °C was the best and was used for more modification and adsorbing process.

2.4 Preparation of carboxylated biochar (BC-CO_2H)

To improve the adsorption performance of biochar, carboxylic functional groups on the biochar surfaces increased according to our previous research [25], and the biochar obtained (2.5 g) was impregnated with HNO_3 (100 mL) at 60 °C for 12 h. Then, the reaction mixture was diluted with deionized water (100 mL), and carboxylated biochar was separated by sequential centrifugation and dried at 60 °C for 10 h.

2.5 Preparation of sulfur nanoparticle-doped biochar (SNPs@BC)

In this experiment, to prepare a thiosulfate solution, $Na_2S_2O_3$ (60 mg) was dissolved in 50 mL deionized. Then, activated biochar (30 mg) was added to the mixture and sonicated for 1 h to yield a biochar-dispersed thiosulfate solution. Then, rosemary extract (10 mL) was added to this solution. Afterward, hydrochloric acid (10%) was added dropwise to the reaction mixture under vigorous stirring for the formation of the sulfur nanoparticles uniformly on the surface of the biochar. The resulting precipitation was centrifugation and washed with deionized water and ethanol. Then, it was dried in a vacuum oven at 40 °C.

2.6 Sorption experiments

The sorption capability of biochar and SNPs@BC was studied with batch sorption experiments. Adsorbents (30 mg) were added to 100 mL of Pb^{2+} (60 ppm) and Cd^{2+} (40 ppm) concentration at ambient temperature, respectively. After stirring in a magnetic stirrer for 12 min, the reaction mixture was filtered immediately, and the supernatant was collected for the measurements. Concentrations of Pb^{2+} and Cd^{2+} in the filtrates were determined using an atomic adsorption spectrophotometer (Perkin Elmer Analyst 400). The adsorbed heavy metal amounts were calculated based on the difference between the initial and final metal concentrations in the supernatant. The adsorbent dosage and solution pH (adjusted by the addition of HCl (0.1 M) or NaOH (0.1 M)) on heavy metal adsorption on SNPs@BC adsorbent were optimized. Solutions without the sorbent were included in the same conditions (concentration, duration, pH, etc.) as controls.

2.7 Seed germination, plant growing, and bioaccumulation

To assay the seed germination, the same number of grass seeds was spread on a filter paper layer moistened with DI water in containers with SNPs@Biochar or SNPs@Biochar + Pb and SNPs@Biochar + Cd (added at the rate of 0.1 g/container, Pb and Cd content 13.57 mg/g). For experiments, l mL of DI water (blank) and 1 mL of lead and cadmium solution of 1.357 mg/mL (containing the same amount of Cd^{2+} and Pb^{2+} as the Cd- and Pb-adsorbed biochar) were applied as a control. Each experiment was performed three times and incubated in the dark at room temperature. Germination percentage was achieved after 72 h and germinal length were determined on the fourth day. In the first step (first 7 days), the growth of seedlings was recorded. The *t*-test one-way ANOVA with a significance level of 95% ($p < 0.05$) was utilized for statistical analyses related to the difference between the numbers of seeds germinated and seedling growing. After 14 days of growth, the harvest of the plants was performed and then washed with water and dried at 105 °C for 30 min. A method like that of Buss et al. was employed to determine the Cd and Pb amounts in the dried plants [23]. First, the dried plants were weighed, and then the samples were heated in a muffle furnace at 550 °C for 10 h. The ashes were digested with a HNO_3:HCl (4:1, v/v) solution. The Cd(II) and Pb(II) amounts in the samples were then determined by ICP-AES and calculated on a dry weight basis.

3 Result and discussion

3.1 Physiochemical properties of BC

In the process of biochar production, the type of biomass and the temperature of the pyrolysis process had a significant effect on some physical and chemical characteristics of biochar [26, 27]. Table 1 shows that the type of biomass and the temperature of the pyrolysis process have a significant effect on some physical and chemical characteristics of biochar. When the temperature of the pyrolysis process increased from 300 to 500 °C, the yield of biochar, cation exchange capacity (CEC), and bulk density decreased, but acidity (pH), electrical conductivity (EC), particle density, stable carbon, total nitrogen, porosity, and specific surface area increased in the prepared biochar.

Based on the obtained results and all the measured parameters, especially the positive aspects of carbon fixation, increasing soil organic matter, and the yield of biochar for the mass and economic production of this material, it could be concluded the biochar obtained from alfalfa residues at a temperature of 500 °C was the best biochar and can improve the physical and chemical properties of the soil and the efficiency of nutrient uptake from the soil, respectively.

3.2 Characterization

The investigation of the surface morphology and dimensions of the SNPs@BC was performed by field emission scanning electron microscopy (FESEM). The FESEM image of SNPs@BC (Fig. 2a, b) shows that the surface of SNPs@BC contained of small flakes. This image also confirmed the porous structure of SNPs@BC that could be derived from the porous structure of raw biomass or was formed during the gasification process.

XRD analysis is an effective characterization technique that confirms the amorphous or crystalline nature of SNPs@BC (Fig. 2c). The peak at $2\Theta = 20–30°$ is related to the stacking structure of aromatic layers (graphite 002). Sharp and non-labeled peaks in SNPs@BC show miscellaneous inorganic components. The main peaks at $2\Theta = 37°$ and 55° are ascribed to the SNPs. The X-ray diffraction peak proved that SNPs@BC has a heterogeneous surface.

Thermogravimetric analysis (TGA) was performed to exhibit the maximum yield of SNPs@BC (Fig. 2d). This maximum biochar yield has a weight loss of 4.33% at 100 °C during the TGA analysis due to the evaporation of moisture/water contained in S-biochar. The rapid weight loss increased significantly to 35.29% between 300 and 400 °C because of the release of the volatiles in SNPs@

Table 1 Physical and chemical analysis of the BC

Temperature	Biochar	(pH)	(EC) ($ds.m^{-1}$)	(CEC) (Cmol. ckg^{-1})	Organic carbon (%)	Organic carbon (%)	Total nitrogen (%)	Porosity (%)	Specific surface area (m^2/g)	Biochar yield (%)	Bulk density (gcm^{-3})	Particle density (gcm^{-3})
300 °C	Wheat residues	6.5	2	78.46	40.36	40.36	3.30	79	32.93	47.3	0.206	0.95
	Alfalfa residues	6	1.7	80.31	42.28	42.28	9.42	62	43.18	59.6	0.399	0.89
	Potato residues	6.7	4	64.34	40.54	40.54	7.75	40	35.47	41.9	0.523	0.87
	Sawdust	6.5	2	60.50	44.22	44.22	4.50	75	43.22	42.5	0.246	1
	Palm tree leaf	7	2.5	75.53	45.63	45.63	4.15	39	40.42	38.1	0.454	0.90
400 °C	Wheat residues	7.4	2.7	60.63	44.71	44.71	5.93	80	40.40	44.9	0.199	0.99
	Alfalfa residues	6.5	2	69.90	56.52	56.52	14.74	72	53.02	55.7	0.338	1.2
	Potato residues	7.5	5	50.32	48.75	48.75	10.03	52	40.23	35.4	0.453	0.94
	Sawdust	7.2	2.5	52.20	60.09	60.09	6.12	87	48.21	35.5	0.200	1.5
	Palm tree leaf	7.5	3.8	62.63	52.67	52.67	7.58	67	47.05	33.6	0.311	0.95
500 °C	Wheat residues	7.6	3.5	42.56	55.94	55.94	6.87	85	44.70	34.5	0.178	1.2
	Alfalfa residues	6.8	2.5	56.22	68.22	68.22	15.68	82	61.14	51.4	0.275	1.5
	Potato residues	7.7	5.2	42.33	65.12	65.12	10.99	65	53.70	30.7	0.349	1
	Sawdust	7.4	3	41.93	67.32	67.32	8.83	89	55.25	26.5	0.185	1.6
	Palm tree leaf	8	4.2	50.55	60.70	60.70	9.32	82	57.16	30.1	0.222	1.2
600 °C	Wheat residues	8	4.1	37.04	57.25	57.25	8.62	87	43.5	32.7	0.182	1.3
	Alfalfa residues	7.2	2.9	49.01	69.02	69.02	15.02	83	61.11	48.7	0.284	1.5
	Potato residues	8.2	5.8	36.90	67.92	67.92	11.04	67	52.25	29.4	0.375	1.2
	Sawdust	7.8	3.5	35.57	68.54	68.54	9.03	89	52.89	25.5	0.186	1.5
	Palm tree leaf	8.4	4.8	47.65	62.07	62.07	9.95	84	58.7	29.2	0.224	1.3

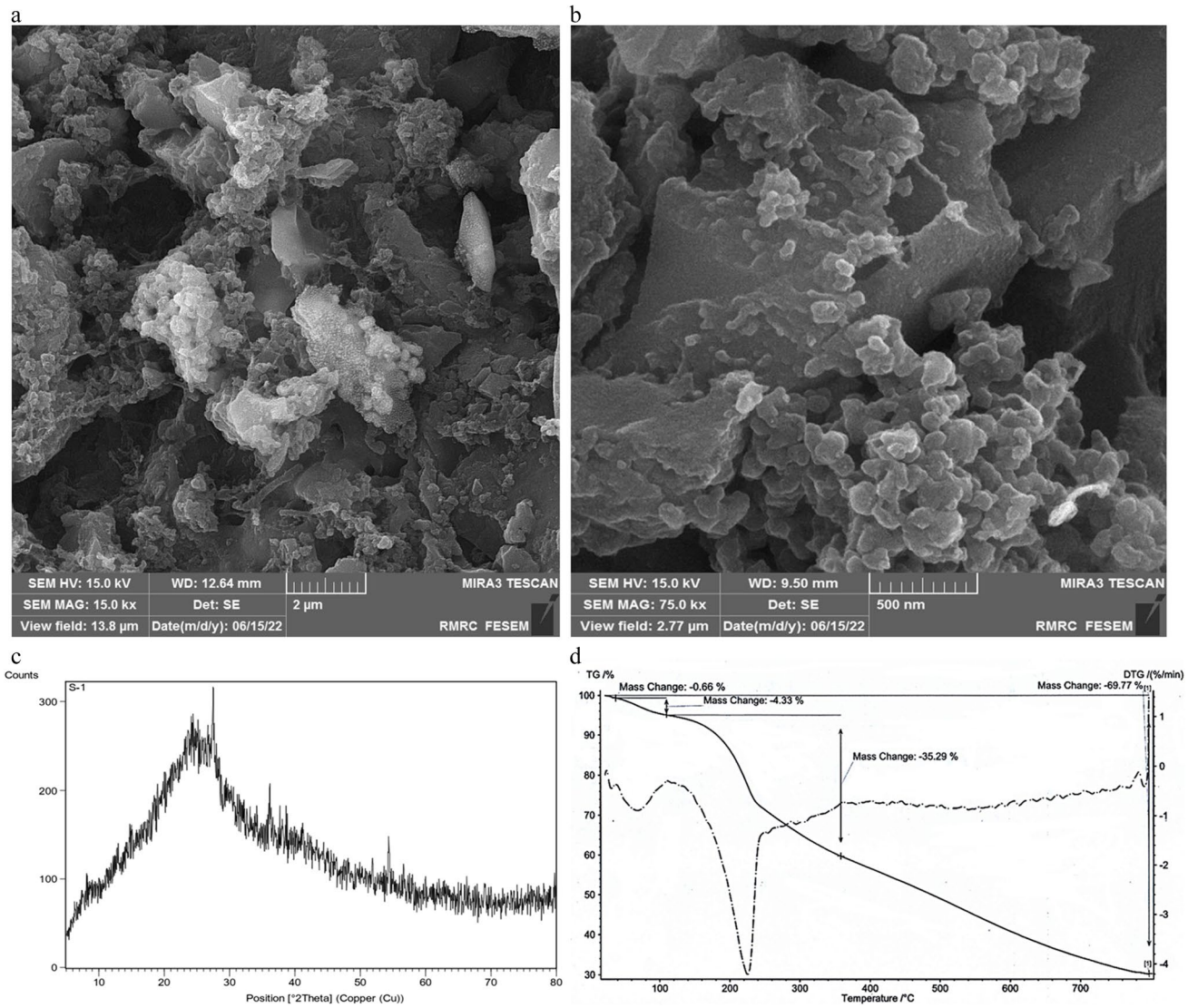

Fig. 2 **a**, **b** FESEM images of SNPs@BC, **c** XRD pattern of SNPs@BC, **d** TGA analysis of SNPs@BC

BC. Subsequently, at 400 to 800 °C, the SNPs@BC sample slowly lost mass due to the decomposition of cellulose and hemicellulose compounds and lignin. Thus, a final residual mass of S-biocarbon of 69.77% was obtained.

The results of the element distribution are shown in Fig. 3a. Elemental mapping of SNPs@BC confirms the correct synthesis of the adsorbent and the broad and homogeneous distribution of the sulfur nanoparticles on the biochar surface. As shown in Fig. 3b, the EDS spectra of SNPs@BC revealed the presence of C (71.76%), N (3.8%), O (6.61%), S (17.11%), and other elements. This high sulfur content on the biochar surface can increase the efficiency of heavy metal uptake.

4 Sorption of heavy metals on modified biochar

4.1 Response surface methodology

The effect of significant parameters on the fabricated system for achieving the best conditions and designing experiments for adsorption of Cd^{2+} and Pb^{2+} was evaluated using response surface methodology (RSM). Central composite design (CCD) is a conventional way of RSM and was utilized for investigation of effective parameters

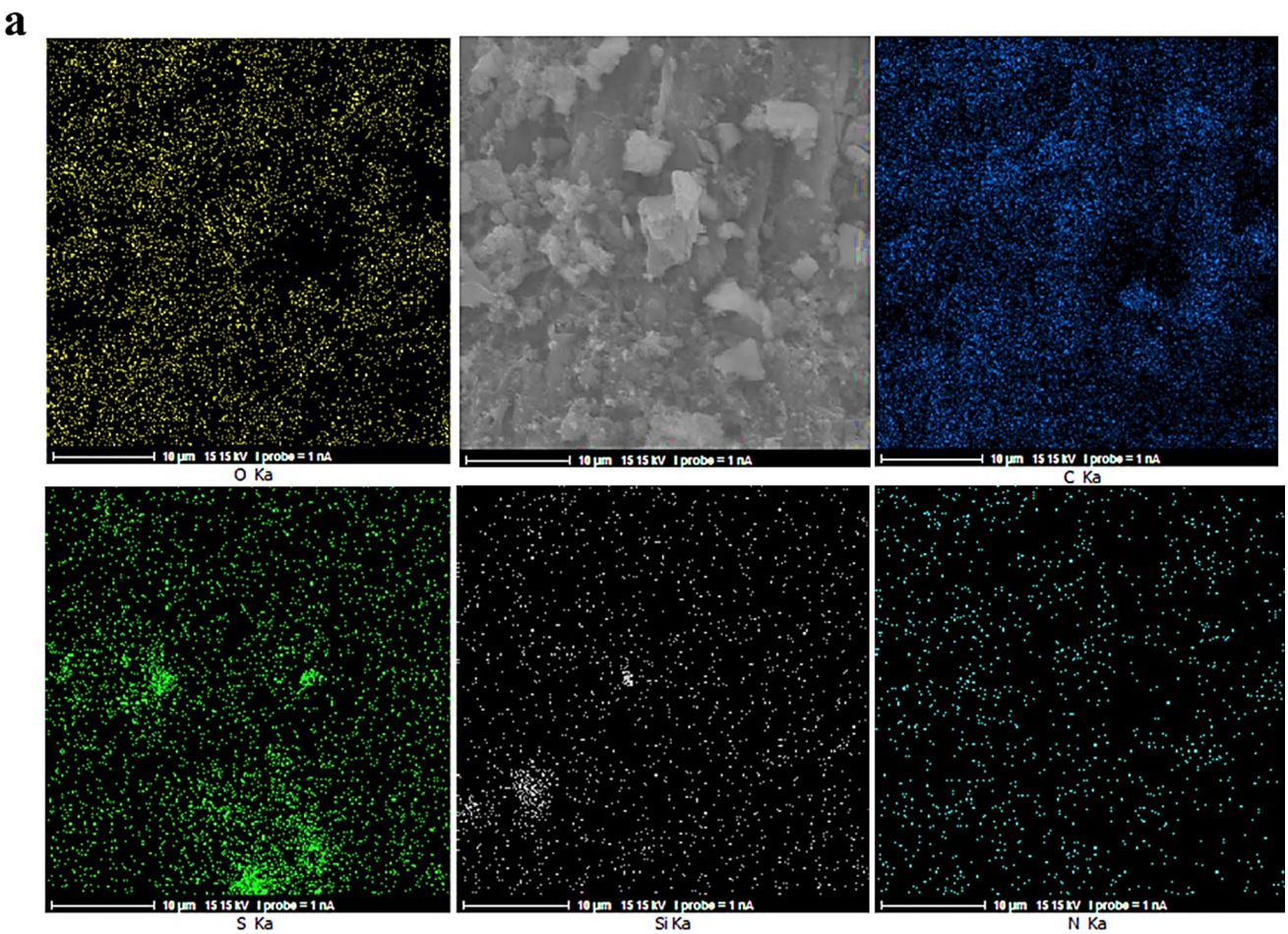

Fig. 3 **a** Elemental mapping and **b** EDS spectrums of the as-prepared SNPs@BC

Table 2 Parameters and their levels in the CCD and experimental dates for Cd^{2+}

Variables	Levels				
	$-\alpha$	Low (−1)	Central (0)	High (+1)	$+\alpha$
(X_1) pH	3.00	4.25	7.00	8.00	6.75
(X_2) Sorbent dose (mg/mL)	5.00	16.25	27.50	38.75	50.00
(X_4) Concentration of Cd^{2+} (ppm)	25.00	10.00	40.00	70.00	55.00
(X_5) Time (min)	5.00	8.75	35.00	18.25	20.00
Run	(X_1)	(X_2)	(X_3)	(X_4)	R
1	4.25	16.25	55.00	16.25	73.47
2	4.25	16.25	25.00	16.25	80.81
3	4.25	38.75	25.00	8.75	86.92
4	5.50	5.00	40.00	12.50	75.23
5	6.75	16.25	55.00	8.75	58.66
6	5.50	27.50	10.00	12.50	68.75
7	5.50	27.50	70.00	12.50	46.11
8	6.75	16.25	55.00	16.25	59.66
9	5.50	27.50	40.00	20.00	97.93
10	5.50	27.50	40.00	12.50	96.87
11	5.50	27.50	40.00	12.50	95.69
12	5.50	27.50	40.00	12.50	97.10
13	5.50	27.50	40.00	5.00	92.82
14	4.25	38.75	35.00	8.75	73.47
15	4.25	38.75	85.00	8.75	79.15
16	5.50	27.50	40.00	12.50	96.13
17	5.50	27.50	40.00	12.50	96.84
18	4.25	38.75	25.00	16.25	87.55
19	6.75	38.75	25.00	16.25	76.42
20	5.50	27.50	40.00	12.50	97.61
21	4.25	38.75	55.00	8.75	66.24
22	6.75	16.256	25.00	8.75	61.73
23	4.25	16.25	85.00	16.25	78.4
24	6.75	38.75	55.00	16.25	70.89
25	4.25	16.25	55.00	8.75	63.32
26	6.75	16.25	25.00	16.25	59.75
27	6.75	38.75	25.00	8.75	77.97
28	3.00	27.50	40.00	12.50	55.78
29	5.50	50.00	40.00	12.50	93.66
30	8.00	27.50	40.00	12.50	40.19

including pH, the concentration of Cd^{2+} and Pb^{2+}, and the mass of sorbent. Based on the full class of CCD, each parameter was studied at five levels ($\pm\alpha, \pm 1, 0$) for decreasing the uncontrollable effects (Table 2 and S2). The total equation for calculating of the number of experimental tests is $N = 2^{K} + 2K + N_o$ (where K is the number of parameters and N_o is the number of central points). Based on this equation, 30 tests were designed which are shown in Table 2 and Table S2. The reproducibility of data and experimental error were determined by using the central points [28, 29]. The estimated result illustrated a good fitting with the second-order polynomial model as follows:

$$Y = b_0 + \sum_{i=1}^{n} b_i X_i + \sum_{i=1}^{n} b_{ii} X_i^2 + \sum_{i=1}^{n-1} \sum_{j=i+1}^{n} b_{ij} X_i X_j + e_i$$

Y is the predicted response; X_i and X_j are independent parameters; n is introduced as the number of parameters; b_i, b_{ii}, and b_{ij} are the linear, quadratic, and interaction coefficients, respectively; and e_i is the residual error [30, 31]. The independent parameters' importance and their interactions at the 95% confidence level were investigated using the analysis of variance (ANOVA). The Fisher test value (F-value) at the p-value < 0.05 was calculated for

Table 3 ANOVA for CCD for Cd^{2+}

Source	Sum of squares	Degree of freedom	Mean square	F-value	*p*-value	
Model	7985.11	14	570.36	402.52	< 0.0001	Significant
X_1	509.68	1	509.68	359.69	< 0.0001	
X_2	469.93	1	469.93	331.64	< 0.0001	
X_3	634.89	1	634.89	448.06	< 0.0001	
X_4	46.26	1	46.26	32.65	< 0.0001	
X_1X_2	67.98	1	67.98	47.98	< 0.0001	
X_1X_3	81.90	1	81.90	57.80	< 0.0001	
X_1X_4	19.67	1	19.67	13.88	0.0020	
X_2X_3	45.56	1	45.56	32.15	< 0.0001	
X_3X_4	36.24	1	36.24	25.58	0.0001	
X_1^2	4069.37	1	4069.37	2871.85	< 0.0001	
X_2^2	257.74	1	257.74	181.89	< 0.0001	
X_3^2	2644.55	1	2644.55	1866.32	< 0.0001	
Residual	21.25	15	1.42			
Lack of fit	18.87	10	1.89	3.96	0.0709	
Pure error	2.38	5	0.48			
Cor total	8006.36	29				Not significant

Table 4 The ANOVA of statistical dates for various models for Cd^{2+}

Model	Std. dev	*p*-value	R^2	Adj-R^2	Pred-R^2	
Linear	15.93	0.1965	0.2405	0.0806	− 0.0859	
2FI[a]	17.91	0.9908	− 0.1618	− 0.2479	− 5.4439	
Quadratic	1.19	< 0.0001	0.9973	0.9949	0.9860	Suggested

determining the corresponding of the model with each parameter.

Based on ANOVA (Table 3 and Table S3), between the linear, two factor interaction, and quadratic model, the quadratic model with the following equation, lowest *p*-value and R^2, adjusted R^2, and predicted R^2 closer to one, was fitted better to the experimental results (Table 4 and Table S4):

$$R = +0.11 - 0.0073X_1 + 0.0057X_2 + 0.055X_3 - 0.0028X_1X_2 - 0.0020X_1X_3 + 0014X_2X_3 - -0.011X_1^2 - 0.00019X_2^2 - 0.008X_3^2$$

4.2 Response surface 3D diagram

The pH is a significant factor that effects on adsorption of heavy metals in an aqueous solution. At highly acidic conditions (pH 2–3), the surface of SNPs@BC saturated with H_3O^+ ions resulting in a strong repulsion between the positive charge of biochar surface and metals cations (Cd^{2+} and Pb^{2+}) and decreasing the uptake of metal ions. In addition, the numerous H_3O^+ ions in the solution create competition with Cd^{2+} and Pb^{2+} ions for the active absorption site on SNPs@BC. With increasing the pH value, the surface of SNPs@BC became negative charge and thus electrostatic interaction between the metal cationic ions and adsorbent surface sites increased. Hence, pH 5.5 was selected as an optimum value for further experiments for both Cd^{2+} and Pb^{2+} ions (Fig. 4a, b and Fig S1a, b).

The modified biochar's zeta potential was measured at pH 6 and resulted in a value of − 37.5 (Fig. S2). This value and its sign are connected to the surface charge of colloidal particles, with a negative surface charge resulting in a negative zeta potential. Research suggests that as the environment becomes more acidic, the surface charge of biochar becomes more positive, reaching − 15. Consequently, the pH_{zpc} of biochar was chosen to be 5.5 [32]. Further findings indicated that the loading of sulfur groups on the biochar surface decreased the pH_{zpc} to approximately 4.7 [33]. As a result, at a pH greater than the pH_{zpc}, the surface of SNPs@BC was negative, strengthening the electrostatic interactions between metal ions and the adsorbent. Conversely, positive charges were created when the pH was less than the pH_{zpc}, due to the protonation of functional groups on the sorbent surface, which weakened the metal ions-adsorbent electrostatic interactions.

The effect of initial Cd^{2+} and Pb^{2+} concentration was investigated on adsorption efficiency. According to the

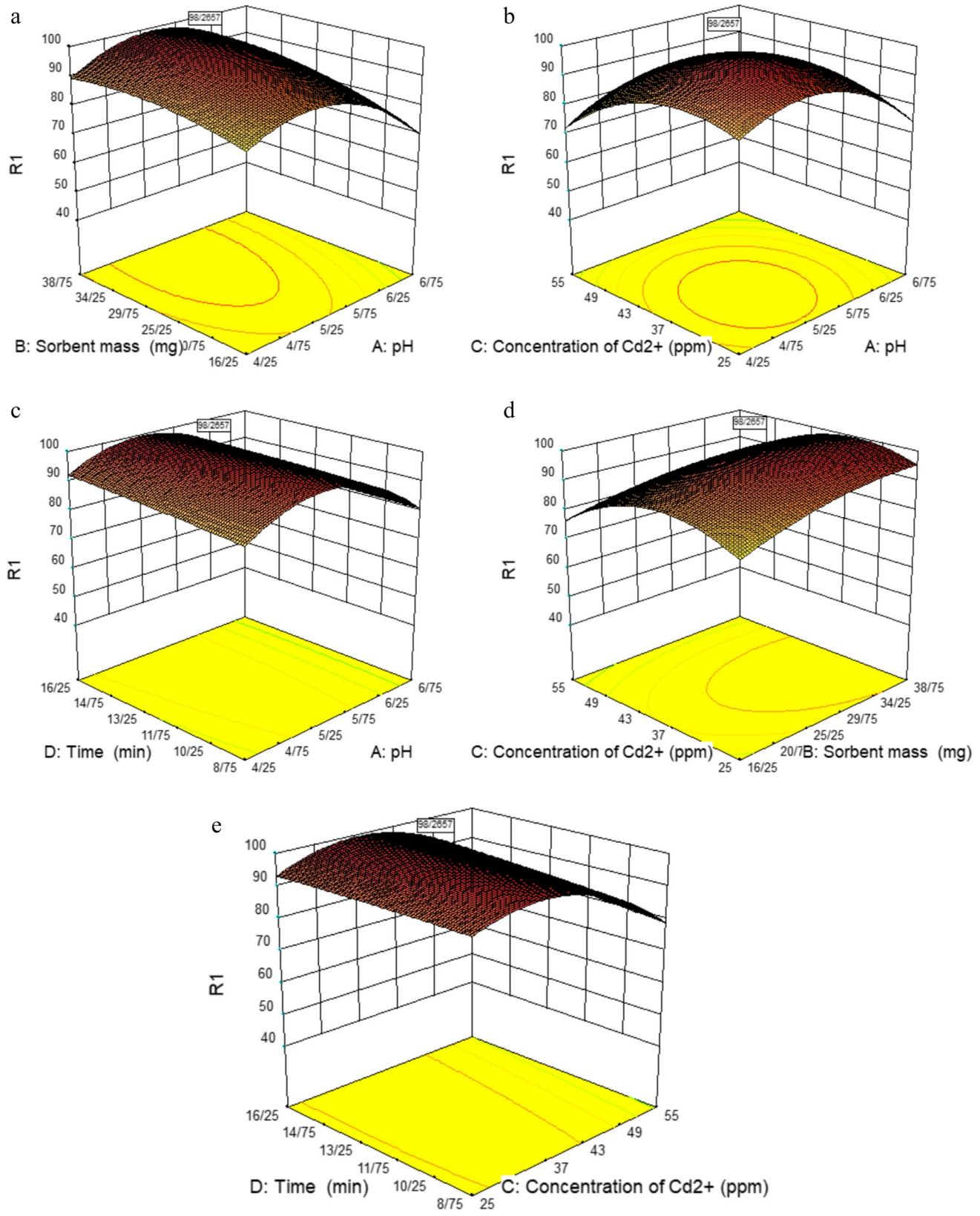

Fig. 4 Response surface 3D diagram for Cd^{2+}

result of Fig. 4b, d and Fig. S1b, d, the maximum adsorption efficiency was achieved at an initial concentration of 40.0 and 60.0 mg/L for Cd^{2+} and Pb^{2+}, respectively. The adsorption efficiency increased with increasing initial concentrations because of the increase in driving force used to the SNPs@BC with an enhancement in the initial Cd^{2+} and Pb^{2+}concentrations.

The amounts of SNPs@BC adsorbent in the adsorption process were evaluated by changing adsorbent amounts in the range of 5.0–50.0 mg. As exhibited in Fig. 4a, d and Fig. S1c, d, the adsorption efficiency for both metal ions increased with S-biochar doses from 27.0 to 30.0 mg for both Cd^{2+} and Pb^{2+}. This increased adsorption efficiency is due to the increase in the number of active and vacant adsorption sites, the enhancement of the distribution coefficient, and the increase of effective interactions between the SNPs@BC and Cd^{2+} and Pb^{2+} ions. However, with higher adsorbent doses than 30.0 mg, the adsorption efficiency was nearly constant, not considerably different from the maximum level.

The effect of contact time on Cd^{2+} and Pb^{2+} ions adsorption is exhibited in Fig. 4c, d and Fig. S1d, e, illustrating that the adsorption of metal ions increased remarkably with time because of the interaction between Cd^{2+} and Pb^{2+} ions with SNPs@BC and the adsorption efficiency achieved about 98.26 and 99.49% within the time of 12 min. The quick initial adsorption can be due to the abundant availability of pores and functional groups on the surface of S-biochar which causes the rapid and easy attaching of Cd^{2+} and Pb^{2+} ions on the surface of S-biochar. However, the adsorption rate decreased gradually because of the decrease of availability of effective sites for occupation and the increased electrostatic repulsion between incoming and adsorbed Cd^{2+} and Pb^{2+} ions.

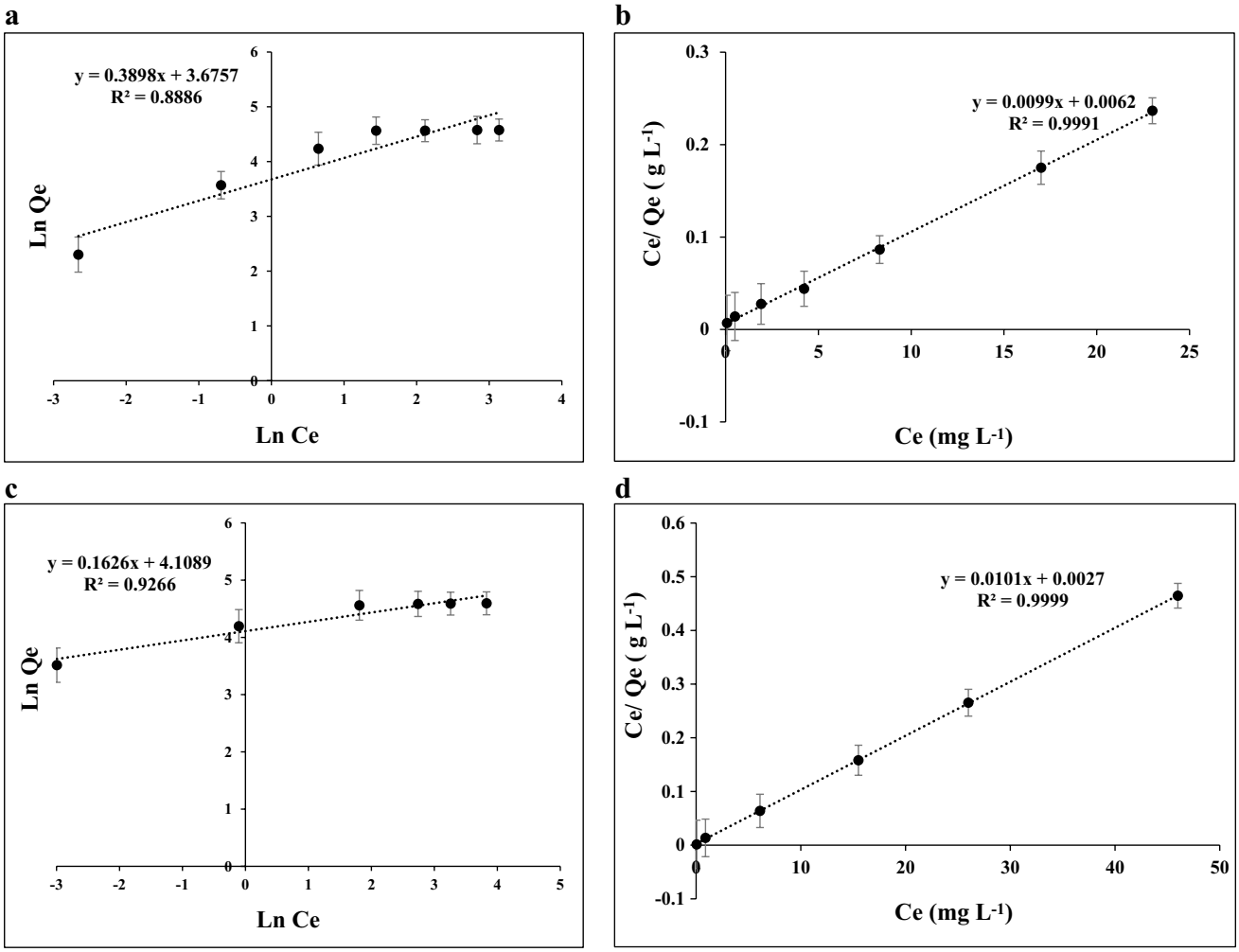

Fig. 5 The linear curve of absorption models onto SNPs@BC

4.3 Adsorption isotherms

In the Cd^{2+} and Pb^{2+} ion adsorption process on SNPs@BC adsorbent, Langmuir and Freundlich were utilized to investigate adsorption isotherms of Cd^{2+} and Pb^{2+} ions by SNPs@BC at initial Cd^{2+} and Pb^{2+} concentrations of 10, 20, 30, 40, 60, and 70 and 10, 30, 50, 60, 80, 110, mg L^{-1} at 25 °C and adsorbent doses of 30.0 mg. Langmuir isotherm described the monolayer and uniform adsorption of the target on the surface of the adsorbent, while the basis of the Freundlich model is the multilayer and heterogeneous adsorption of the target on the adsorbent. The Langmuir and Freundlich isotherms follow Eqs. 1 and 2, respectively, and their curves are shown in Fig. 5.

$$\log\ Q_e = \log\ K_f + \frac{1}{n}\log\ C_e \tag{1}$$

$$\frac{C_e}{q_e} = \frac{1}{K_{lq_{max}}} + \frac{C_e}{q_{max}} \tag{2}$$

where C_e is the Cd^{2+} and Pb^{2+} equilibrium concentration (mg/g) and Q_{max} is the maximum adsorption (mg/g). K_L is the equilibrium constant of the Langmuir Eq. (1/mg), while K_f is the Freundlich constant (mg/g) [29, 30].

The Langmuir model has a higher correlation coefficient (R^2) and SD than that of the Freundlich model, showing the experimental date fitted better to the Langmuir model and Cd^{2+} and Pb^{2+} adsorption on the entire SNPs@BC surface is monolayer and uniform (Table 5, Fig. 5).

Table 5 Kinetic constants of different models for Cd^{2+} and Pb^{2+} ions adsorption to the SNPs@BC

Isotherm models	Parameters	Value
Langmuir (Cd^{2+})	Q_{max} (mg g^{-1})	97.0
	K_b (L mg^{-1})	3.82
	R^2	0.9998
	SD	3.8
Freundlich (Cd^{2+})	K_f (mg g^{-1})	60.88
	n	6.15
	R^2	0.9266
	SD	4.7
Langmuir (Pb^{2+})	Q_{max} (mg g^{-1})	99.0
	K_b (L mg^{-1})	1.60
	R^2	0.9992
	SD	4.3
Freundlich (Pb^{2+})	K_f (mg g^{-1})	39.47
	n	2.56
	R^2	0.8886
	SD	5.1

Table 6 Comparison of adsorption capacities of the various adsorbent for removal of Pb and Cd ions

Adsorbent	qm (mg.g-1)		Ref
	Pb(II)	Cd(II)	
Fe2O3/Oak bark biochar	30.2	7.4	34
BC300	50.41	23.64	35
peanut hull biochar	50.05	6.36	36
banana peels	2.18	5.71	37
cron straw biochar	28.99	38.91	38
mango peel waste	99.0	68.92	39
SNPs@BC	97	99	This study

A comparison of the values of the Langmuir isotherm parameter Q_{max} obtained in this study with those reported in previous studies for the sorption of Cd(II) and Pb(II) ions from aqueous solutions using adsorbents was also carried out and are presented in Table 6 and showed.

4.4 Absorption mechanism

The absorption mechanism of Cd^{2+} and Pb^{2+} ions by the SNPs@BC adsorbent is exhibited in Fig. 6, and the

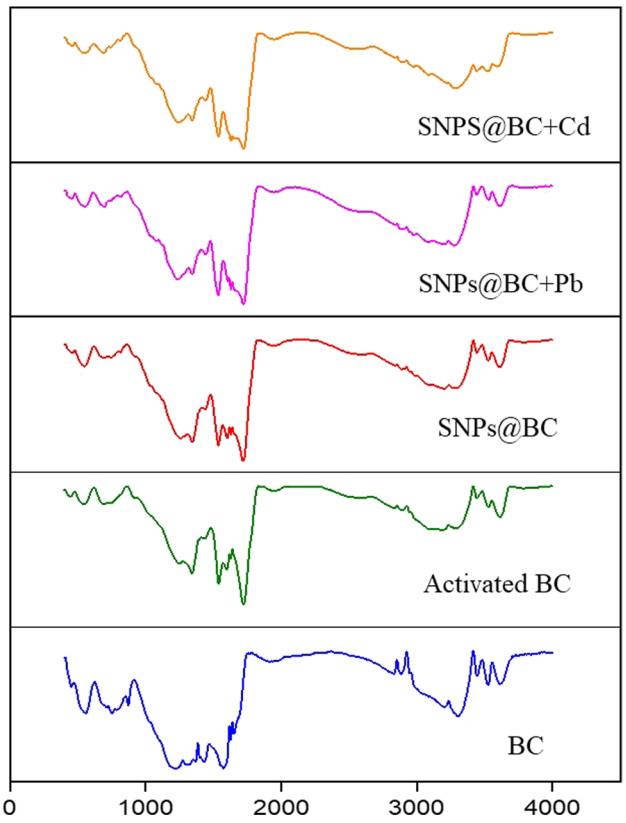

Fig. 6 FT-IR spectrum of BC, activated BC, SNPs@BC, SNPs@BC + Pb, and SNPs@BC + Cd

FT-IR of SNPs@BC before and after absorption of Cd^{2+} and Pb^{2+} ions is compared in Fig. 6. The broad peak at 3100–3200 cm^{-1} is related to stretching vibration of the OH. The peaks at 1650 cm^{-1} are ascribed to the stretching vibration of carbocyclic groups, the peak at 1540 cm^{-1} is related to the stretching vibration of C = O, and the carbonyl group and the peak at 1803 are attributed to the aromatic C–H. After the modification of biochar with SNPs, the peak of the bending vibration of C = O and COOH groups became weaker, and the aromatic C-H peak did not observe. In addition, the peak at 553 cm^{-1} is appeared and related to the asymmetric stretching of sulfate on SO_3^{2-}. Carboxylate is polar and can accept and donate both H^+ and OH^- ions because of the presence of carbonyl and hydroxyl groups. The complex can be formed between Cd^{2+} and Pb^{2+} ions and carboxylic groups by replacing H^+ with Cd^{2+} and Pb^{2+} ions. Obviously, the peak intensity of the O–H stretching vibration band at 3100–2300 cm^{-1} decreased and shifted to a lower wavelength and the peak of carboxylic groups at 1650 cm^{-1} shifted to 1645 and 1643 cm^{-1} for Cd^{2+} and Pb^{2+}, respectively, which confirms the successful formation of the complex between Cd^{2+} and Pb^{2+} ions and the functional groups of SNPs@BC.

4.5 Seed germination, early growth, and bioaccumulation

The comparison of results illustrated that the average seedling length in the control groups SNPs@BC, SNPs@BC + Pb, and SNPs@BC + Cd were, respectively, (32 mL), (22 mL), (21 mL), and (20 mL) which did not reach statistical significance. Seedling length measurements in soluble lead and cadmium groups were (11 mL) and (12 mL), respectively, and these two groups in comparison to the control groups, SNPs@BC, SNPs@BC + Pb, and SNPs@BC + Cd in terms of seedling length had statistically significant differences (Figs. 7, 8, and 9). The results showed that the average germination rates in soluble lead and cadmium groups were 90% and 90%, respectively, which was almost similar to the control groups, SNPs@BC, SNPs@BC + Pb, and SNPs@BC + Cd, and they showed no statistically significant difference. The results of elemental analysis illustrated that high

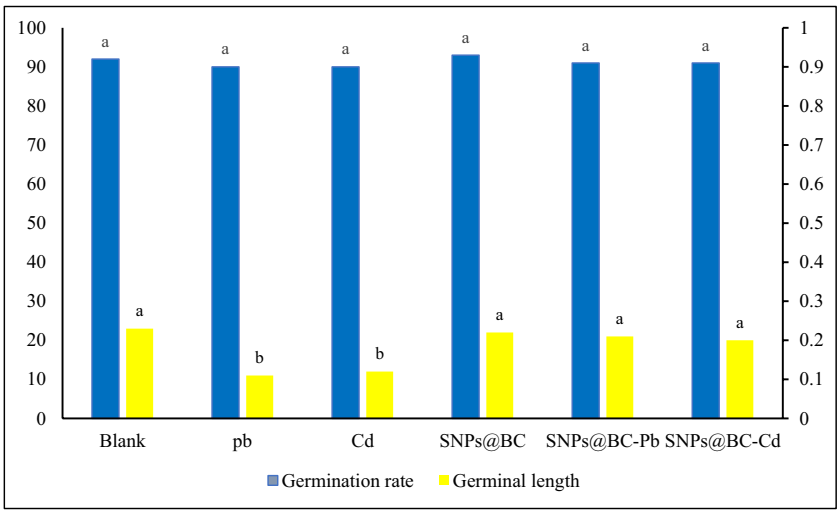

Fig. 7 Comparison of the average biological effects of soluble lead (Pb), soluble cadmium (Cd), biochar modified with SNPs (SNPs@BC), biochar modified with SNPs loaded with lead (SNPs@BC + Pb), and biochar modified with SNPs loaded with cadmium (SNPs@BC + Cd) on germination rate and seedling length

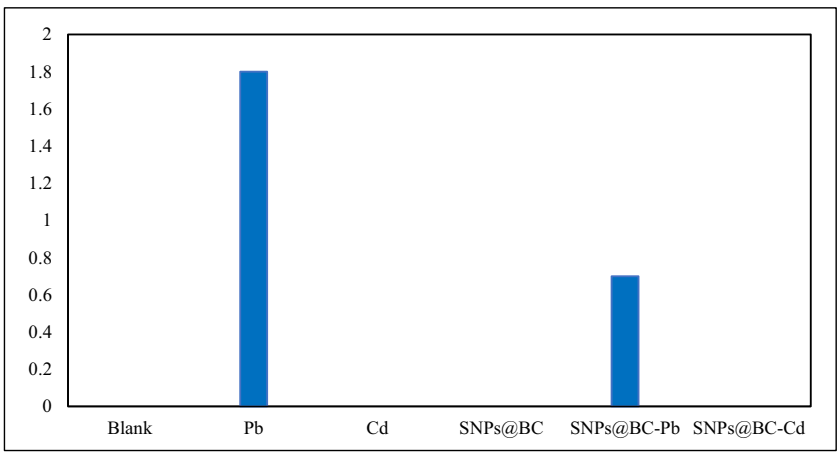

Fig. 8 Biological effects of soluble lead (Pb), soluble cadmium (Cd), biochar modified with SNPs (SNPs@BC), biochar modified with SNPs loaded with lead (SNPs@BC + Pb), and biochar modified with SNPs loaded with cadmium (SNPs@BC + Cd)

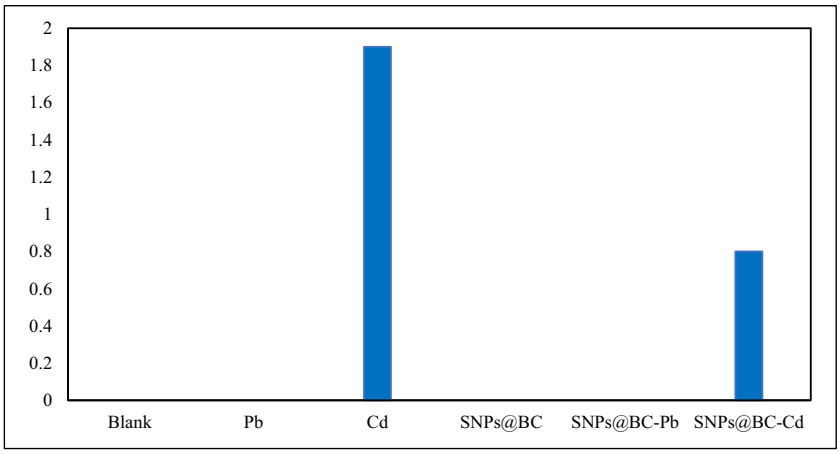

Fig. 9 Biological effects of soluble lead (Pb), soluble cadmium (Cd), biochar modified with SNPs (BB-S), biochar modified with SNPs loaded with lead (SNPs@BC + Pb), and biochar modified with SNPs loaded with cadmium (SNPs@BC + Cd)

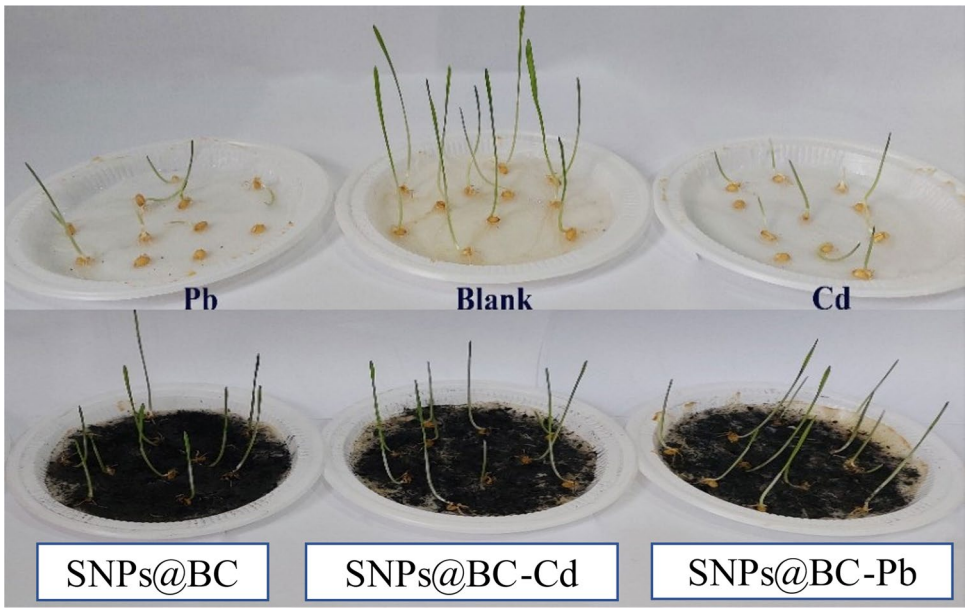

Fig. 10 Photo of seedling on day 7 under the biological effects of blank, soluble lead (Pb), soluble cadmium (Cd), biochar-modified SNPs (SNPs@BC), biochar modified with SNPs filled with lead (SNPs@BC + Pb), and biochar modified with SNPs filled cadmium (SNPs@BC + Cd)

levels of lead and cadmium were found in the soluble lead (1.8 mg/g) and soluble cadmium (1.9 mg/g) groups, respectively, while in SNPs@BC + Pb and SNPs@BC + Cd, the amount of lead and cadmium was 0.7 mg/g and 0.8 mg/g, respectively (Fig. 7, 8, 9 and 10), and in the control and SNPs@BC groups, it was very insignificant, and undetectable (ICP-AES) detection limit was less than 0.01 mg/L. The results of germination, growth, and absorption tests showed that biochar modified with SNPs can decrease the toxicity of heavy metals and can be added to soil as a remedial agent in soils which are contaminated with these metals.

5 Conclusion

Activated biochar doped with sulfur nanoparticles was synthesized for the first time and employed as an efficient biosorbent for the adsorption of Cd^{2+} and Pb^{2+} ions from aqueous solutions. This adsorbent also has the ability to decrease the toxicity of heavy metals to plants. The effect of four significant parameters including pH, initial Cd^{2+} and Pb^{2+} concentrations, adsorption dose, and interaction time was studied and optimized by CCD based on RSM. The significant parameters in the adsorption process were determined by ANOVA. The quadratic was the best model. Under optimum conditions, the adsorption efficiency was obtained 98.26% and 99.49% for Cd^{2+} and Pb^{2+}, respectively. The adsorption process can well correspond with the Langmuir adsorption isotherm. Based on the findings, SNPs@BC as a low cost and alternative adsorbent possesses a high potential and capacity for the adsorption of Cd^{2+} and Pb^{2+} ions from aqueous solutions and remediation of soil.

Supplementary Information The online version contains supplementary material available at https://doi.org/10.1007/s13399-023-05021-y.

Acknowledgements The authors express appreciation to the University of Jiroft Faculty Research Committee for supporting this investigation.

Author contribution NS: conceptualization, supervision, and analyzed the data, authored, or reviewed drafts of the manuscript. MA: performed the experiments, analyzed the data, contributed reagents/materials/analysis tools, and prepared Figs. 7, 8, 9, 10 and Table 1. NSM: performed the experiments. RA: conceived and designed the experiments, prepared Figs. 1, 2, 3, 4, 5, 6 and Tables 1, 2, 3, 4, 5, and authored and reviewed drafts of manuscript. MJ: authored and reviewed drafts of the paper. MAN: authored and reviewed drafts of the paper.

Funding The authors have not disclosed any funding.

Data availability The data supporting this research is provided in the manuscript.

Declarations

Ethics approval This article does not include any studies with either humans or animals conducted by any of the authors. We did not gather any specimens of both humans and animals.

Conflict of interest The authors declare no competing interests.

References

1. Barsbay M, Kavaklı PA, Tilki S, Kavaklı C, Güven O (2018) Porous cellulosic adsorbent for the removal of Cd (II), Pb (II) and Cu (II) ions from aqueous media. Radiat Phys Chem 142:70–76
2. Chen G, Shi L (2017) Removal of Cd (II) and Pb (II) ions from natural water using a low-cost synthetic mineral: behavior and mechanisms. RSC Adv 7:43445–43454
3. Amarasinghe BM, Williams RA (2007) Tea waste as a low-cost adsorbent for the removal of Cu and Pb from wastewater. J Chem Eng 132:299–309
4. Chen G, Shi L (2017) Removal of Cd (II) and Pb (II) ions from natural water using a low-cost synthetic mineral: behavior and mechanisms. RSC Adv 7:43445–43454
5. Hayat MT, Nauman M, Nazir N, Ali S, Bangash N (2019) Environmental hazards of cadmium: past, present, and future. Cadmium toxicity and tolerance in plants. Academic Press, pp 163–183
6. Chen G, Shah KJ, Shi L, Chiang PC (2017) Removal of Cd (II) and Pb (II) ions from aqueous solutions by synthetic mineral adsorbent: performance and mechanisms. Appl Surf Sci 1:296–305
7. Qu J, Zhang X, Liu S, Li X, Wang S, Feng Z, Wu Z, Wang L, Jiang Z, Zhang Y (2022) One-step preparation of Fe/N co-doped porous biochar for chromium (VI) and bisphenol a decontamination in water: insights to co-activation and adsorption mechanisms. Biores Technol 1(361):127718
8. Qu J, Li Z, Bi F, Zhang X, Zhang B, Li K, Wang S, Sun M, Ma J, Zhang Y (2023) A multiple Kirkendall strategy for converting nanosized zero-valent iron to highly active Fenton-like catalyst for organics degradation. Proc Natl Acad Sci 120(39):e2304552120
9. Eloussaief M, Benzina M (2010) Efficiency of natural and acid-activated clays in the removal of Pb (II) from aqueous solutions. J Hazard Mater 178:753–757
10. Ding Y, Liu Y, Liu S, Li Z, Tan X, Huang X, Zeng G, Zhou Y, Zheng B, Cai X (2016) Competitive removal of Cd (II) and Pb (II) by biochars produced from water hyacinths: performance and mechanism. RSC adv 6:5223–5232
11. Chen ZL, Zhang JQ, Huang L, Yuan ZH, Li ZJ, Liu MC (2019) Removal of Cd and Pb with biochar made from dairy manure at low temperature. J Integr Agric 18:201–210
12. Zhou Y, Gao B, Zimmerman AR, Fang J, Sun Y, Cao X (2013) Sorption of heavy metals on chitosan-modified biochars and its biological effects. J Chem Eng 231:512–518
13. Yao Y, Gao B, Inyang M, Zimmerman AR, Cao X, Pullammanappallil P, Yang L (2011) Removal of phosphate from aqueous solution by biochar derived from anaerobically digested sugar beet tailings. J Hazard Mater 190:501–507
14. Inyang M, Gao B, Ding W, Pullammanappallil P, Zimmerman AR, Cao X (2011) Enhanced lead sorption by biochar derived from anaerobically digested sugarcane bagasse. Separ Sci Technol 46:1950–1956
15. Zhang M, Gao B, Yao Y, Xue Y, Inyang M (2012) Synthesis, characterization, and environmental implications of graphene-coated biochar. Sci Total Environ 435:567–572
16. Xue Y, Gao B, Yao Y, Inyang M, Zhang M, Zimmerman AR, Ro KS (2012) Hydrogen peroxide modification enhances the ability of biochar (hydrochar) produced from hydrothermal carbonization of peanut hull to remove aqueous heavy metals: batch and column tests. Chem Eng J 200:673–680
17. Zhang W, Wang L, Sun H (2011) Modifications of black carbons and their influence on pyrene sorption. Chemosphere 85:1306–1311
18. Jawhid O, Seyedi N, Zohuri GH, Ramezanian N (2021) Cellulose Schiff base as a bio-based polymer ligand: extraction, modification and metal adsorption study. J Polym Environ 29:1860–1868
19. Beesley L, Moreno-Jiménez E, Gomez-Eyles JL, Harris E, Robinson B, Sizmur T (2011) A review of biochars' potential role in the remediation, revegetation and restoration of contaminated soils. Environ Pollut 159:3269–3282
20. Chen Y, Liang W, Li Y, Wu Y, Chen Y, Xiao W, Zhao L, Zhang J, Li H (2019) Modification, application and reaction mechanisms of nano-sized iron sulfide particles for pollutant removal from soil and water: a review. J Chem Eng 362:144–159
21. Cao X, Ma L, Liang Y, Gao B, Harris W (2011) Simultaneous immobilization of lead and atrazine in contaminated soils using dairy-manure biochar. Environ Sci Technol 45:4884–4889
22. Uchimiya M, Klasson KT, Wartelle LH, Lima IM (2011) Influence of soil properties on heavy metal sequestration by biochar amendment: 1. Copper sorption isotherms and the release of cations. Chemosphere 82:1431–1437
23. Hamed H, Boulila S, Ghrab F, Kallel R, Boudawara T, El Feki A (2020) The preventive effect of aqueous extract of rosemary (Rosmarinus officinalis) leaves against the nephrotoxicity of carbon tetrachloride in mice. Arch Physiol Biochem 126:201–208
24. Zahedifar M, Seyedi N, Shafiei S, Basij M (2021) Surface-modified magnetic biochar: highly efficient adsorbents for removal of Pb (II) and Cd (II). Mater Chem Phys 271:124860
25. Sun Y, Xiong X, He M, Xu Z, Hou D, Zhang W, Ok YS, Rinklebe J, Wang L, Tsang DC (2021) Roles of biochar-derived dissolved organic matter in soil amendment and environmental remediation: a critical review. J Chem Eng 424:130387
26. Wang J, Wang S (2019) Preparation, modification and environmental application of biochar: a review. J Clean Prod 227:1002–1022
27. Afsharipour R, Dadfarnia S, Shabani AM, Kazemi E, Pedrini A, Verucchi R (2021) Fabrication of a sensitive colorimetric nanosensor for determination of cysteine in human serum and urine samples based on magnetic-sulfur, nitrogen graphene quantum dots as a selective platform and Au nanoparticles. Talanta 226:122055
28. Afsharipour R, Shabani AM, Dadfarnia S (2022) A selective off–on fluorescent aptasensor for alpha-fetoprotein determination

based on n-carbon quantum dots and oxidized nanocellulose. J Photochem Photobiol A: Chem 428:113872
29. Dil EA, Ghaedi M, Asfaram A, Goudarzi A (2015) Synthesis and characterization of ZnO-nanorods loaded onto activated carbon and its application for efficient solid phase extraction and determination of BG from water samples by micro-volume spectrophotometry, New. J Chem 39:9407–9414
30. Kyzas GZ, Nanaki SG, Koltsakidou A, Papageorgiou M, Kechagia M, Bikiaris DN, Lambropoulou DA (2015) Effectively designed molecularly imprinted polymers for selective isolation of the antidiabetic drug metformin and its transformation product guanylurea from aqueous media. Anal Chim Acta. 866:27–40
31. Yuan JH, Xu RK (2011) The amelioration effects of low temperature biochar generated from nine crop residues on an acidic Ultisol. Soil Use Manag 27:110–115
32. Liu R, Zhang Y, Hu B, Wang H (2022) Improved Pb (II) removal in aqueous solution by sulfide@ biochar and polysaccharose-FeS@ biochar composites: efficiencies and mechanisms. Chemosphere 287:132087
33. Nasseh N, Barikbin B, Taghavi L, Nasseri MA (2019) Adsorption of metronidazole antibiotic using a new magnetic nanocomposite from simulated wastewater (isotherm, kinetic and thermodynamic studies). Compos B Eng 159:146–156
34. Nasiri A, Rajabi S, Hashemi M (2022) CoFe2O4@ methylcellulose/AC as a new, green, and eco-friendly nano-magnetic adsorbent for removal of reactive red 198 from aqueous solution. Arab J Chem 15:103745
35. Ahmad M, Rajapaksha AU, Lim JE, Zhang M, Bolan N, Mohan D, Vithanage M, Lee SS, Ok YS (2014) Biochar as a sorbent for contaminant management in soil and water: a review. Chemosphere 99:19–33
36. Zl C, Jq Z, Huang L, Yuan Zh, Zj Li, Mc L (2019) Removal of Cd and Pb with biochar made from dairy manure at low temperature. J Integr Agric 18(1):201–210
37. Cui LQ, Yan JL, Li LQ, Quan GX, Ding C, Chen TM, Yin CT, Gao JF, Hussain Q (2015) Does biochar alter the speciation of Cd and Pb in aqueous solution? Bioresour 10(1):88–104
38. Anwar J, Shafique U, Salman M, Dar A, Anwar S (2010) Removal of Pb(II) and Cd(II) from water by adsorption on peels of banana. Bioresour Technol 101(6):1752–1755
39. Chi T, Zuo J, Liu F (2017) Performance and mechanism for cadmium and lead adsorption from water and soil by corn straw biochar. Front Environ Sci Eng 11:1–8